Frequency response function identification using fused filament fabrication-3D-printed embedded ArUco markers

Lorenzo Capponi[1], Tommaso Tocci[2], Giulio Tribbiani[2], Massimiliano Palmieri[2], Gianluca Rossi[2]

[1] *Aerospace Department, University of Illinois at Urbana-Champaign, 61801 Urbana, Illinois*
[2] *Engineering Department, University of Perugia, 06122 Perugia, Italy*

ABSTRACT
The assessment of modal components is a fundamental step in structural dynamics. While experimental investigations are generally performed through full-contact techniques, using accelerometers or modal hammers, this research proposes a non-contact Frequency Response Function identification measurement technique based on ArUco square fiducial markers displacement detection. A video of the phenomenon to be analyzed is acquired, and the displacement is measured through markers, using a dedicated tracking algorithm. The proposed method is presented using a harmonically excited fused filament fabrication-3D-printed flexible structure, equipped with multiple embedded-printed markers, whose displacement is measured with an industrial camera. Comparison with numerical simulation and an established experimental approach is finally provided for the results validation.

Corresponding author: Lorenzo Capponi, e-mail: lcapponi@illinois.edu

1. INTRODUCTION

When a flexible structure is excited at or close to one of its natural frequencies, resonance phenomenon occurs [1], [2]. In resonance operating conditions, most of the energy is released and the response vibration amplitudes significantly increases. This process generally leads to an increasing of the vibration fatigue damage [3]-[5]. Due to this, the determination of the modal components (i.e., natural frequencies, mode shapes and damping) is fundamental in any structural dynamics approach, either numerical or experimental, in order to avoid potential critical conditions [2]. With this perspective, many experimental approaches have been developed in years that allows the determination of modal components [6]-[8]. The impact excitation using modal hammers and the shaker excitation are the two most used full-contact experimental approaches [2], [9]. In the last years, many image-based analysis have been introduced for the displacement measurements [10], [11] and consequently for the structural dynamics due to several operating advantages, e.g. high spatial density, full-field information, no sensors to be placed on the structure [12]. Javh et al. [13] proved the hybrid modal-parameter identification of full-field mode shapes using a

DSLR camera for responses far above the camera's frame rate, employing the Lucas-Kanade Optical Flow algorithm [14]. Gorjup et al. [15] researched on the full-field 3D Operating-Deflection-Shape (ODS) identification using the frequency domain triangulation in the visible spectrum. Capponi et al. [16] proposed a methodology based on the thermoelastic principle for the visual modal strain determination, that allowed the fatigue modal damage identification.

One of the most promising approaches for deformation, displacement and motion detection involves markers, either physical or virtual [17]-[19]. Virtual markers are often employed as they allow tracking objects in subsequent acquired frames without introducing physical targets [20], [21]. When virtual markers are not available, physical markers are employed [22], [23], and among them, the ArUco marker library (ArUco - Augmented Reality University of Cordoba) was found to be one of the most effective and robust to detection errors and occlusion [24]-[26]. Elangovan et al. [27] used them for decoding contact forces exerted by adaptive hands, while Sani and Karamian [28] and Lebedev et al. [29] employed them for drone quadrotor and UAV autonomous navigation and landing, respectively. In relation to the use of fiducial markers for vibrations measurement, Abdelbarr et al. [30] researched

structural 3D displacement using ArUco markers, while the study of Kalybek et al. [31] provides one of the first evidence of the capability of optical vibration monitoring systems in modal identifications. Recently, Tocci et al. [32] presented an ArUco marker-based vibration displacement technique, provided with an uncertainty analysis, based on acquisition parameters influence investigation.

In this research, the ArUco markers are employed for the determination of the Frequency Response Function (FRF) of a flexible structure using image-based analysis. In this study, the growing potential of 3D printing is exploited: the tested structure is realised in Polylactic Acid using Fused Filament Fabrication 3D printing methodology. The employed markers are still realised using 3D printing methodology and they are generated as embedded in the structure during a unique printing job. An established experimental FRF assessment technique and a numerical model are also provided for the results validation.

The manuscript is organized as follows. In Sec. 2 the theoretical background of structural dynamics and marker detection is given. In Sec. 3, the proposed approach is presented and in Sec. 4 the experimental campaign and the numerical model are described. Sec. 5 gives the results while Sec. 6 draws the conclusions.

2. THEORETICAL BACKGROUND

2.1. Structural dynamics

Flexible structures can be represented by N-degrees of freedom (DOFs) systems using [8]:

$$M\ddot{x}(t) + D\dot{x}(t) + Kx(t) = D\dot{y}(t) + Ky(t), \tag{1}$$

where M, D and K are the mass, damping and stiffness matrices, while $y(t)$ and $x(t)$ are the excitation and the response displacements of the DOFs, respectively. Assuming a harmonic excitation $y(t) = Ye^{i\omega t}$ and a response $x(t) = Xe^{i\omega t}$, Eq. (1) can be written as[8]:

$$(-\omega^2 + i\omega DM^{-1} + KM^{-1})X(\omega) = (i\omega DM^{-1} + KM^{-1})Y(\omega). \tag{2}$$

From Eq. (2), the displacement-response amplitude is obtained as [8]:

$$\alpha(\omega) = \frac{X(\omega)}{Y(\omega)} = \frac{i\omega DM^{-1} + KM^{-1}}{-\omega^2 + i\omega DM^{-1} + KM^{-1}} \tag{3}$$

where $\alpha(\omega)$ defines the receptance matrix, that is also know as the Frequency-Response Function (FRF) from displacement to displacement [2], [8]. Using the eigenvalues notation, $\alpha(\omega)$, which relates the j-th response to the k-th excitation, can be written as [2], [8]:

$$\alpha_{jk}(\omega) = \sum_{r=1}^{N}\left(\frac{{}_rR_{jk}}{i\omega - \lambda_r} + \frac{{}_rR*_{jk}}{i\omega - \lambda*_r}\right), \tag{4}$$

where r is the eigenvalue index (i.e., the mode index), * stands for the complex conjugate notation, ${}_rR_{jk}$ is the modal constant and λ_r is r-th eigenvalue [2].

In the experimental modal analysis, several approaches for the excitation and the measurement of the structural dynamics can be employed [2]. The Frequency Response Function of a system can be experimentally determined using FRF estimators [8]. When there is no input noise and the output noise is uncorrelated, the $\hat{\alpha}(\omega)$ is used:

$$\hat{\alpha}(\omega) = \frac{\widehat{S_{yx}}(\omega)}{\widehat{S_{yy}}(\omega)} \tag{5}$$

where $\widehat{S_{yx}}(\omega)$ is the cross-spectrum between the input excitation y and the output response x and $\widehat{S_{yy}}(\omega)$ is the auto-spectrum of the input excitation y (the ^ symbol denotes the estimation from measurements), defined as:

$$\widehat{S_{yx}}(\omega) = \frac{1}{T}[\widehat{Y^*}(\omega)\,\hat{X}(\omega)], \tag{6}$$

$$\widehat{S_{yy}}(\omega) = \frac{1}{T}[\widehat{Y^*}(\omega)\,\hat{Y}(\omega)] \tag{7}$$

where T is the measurement time length, $\hat{Y}(\omega)$ and $\hat{X}(\omega)$ are the spectra of the input excitation and of the response, respectively.

For the experimental FRF reconstruction, the modal parameters identification is required, and, for this purpose, different methods can be used [33], [34]. The preferred procedure in experimental modal analysis consists of using the Least Square Frequency Domain (LSFD) approach for the modal constants identification from the eigenvalues $\hat{\lambda}_r$ obtained through the Least Square Complex Frequency (LSCF) and the stabilisation chart [35].

2.2. ArUco marker detection

An ArUco marker is a square-marker composed by a wide black border, that facilitates its detection in the image, and an inner binary-matrix, which determines its identification number [24], [25]. An example of ArUco marker is presented in Figure 1.

The identification of an ArUco marker in a captured frame requires several computational steps [32], that, as well as for the generation of the marker, are provided from the OpenCV Python dedicated library. However, properly developed image-processing (e.g., filters and thresholds) can facilitate the pattern recognition. The marker detection is based on its 4 corners identification in each captured frame (see Figure 1). From the corners, the spatial coordinates of the centre of the marker (x_c, y_c) are evaluated frame-by-frame during the acquisition [32]:

$$C = (x_c, y_c) = \vec{G} \cdot \left(\frac{1}{4}\sum_{r=1}^{4}|x_r|, \frac{1}{4}\sum_{r=1}^{4}|y_r|\right) \tag{8}$$

where (x_r, y_r) are the coordinates of the r-th vertex and $\vec{G}$ is the calibration factor from pixel units to SI units, defined as the ratio between the side length of the physical marker in SI units d_{SI} and
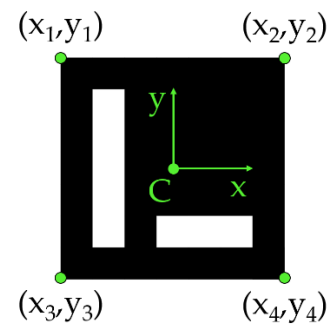
Figure 1. Example of an ArUco marker from *Original* dictionary: corners and reference system.

the average of the four side lengths (in pixels) of the captured marker in the FOV $\overrightarrow{d_{px}}$:

$$\vec{G} = d_{SI} \ / \ \overrightarrow{d_{px}} \quad \text{[m/pixels]}. \tag{9}$$

The calibration factor is evaluated at each new acquired frame. In this way, if the marker is subjected to non-planar displacements or deformations during the measurement, the calibration factor is again estimated. The time-history of the centre the marker $C(t)$ is obtained by tracking it during the acquisition.

3. ARUCO MARKER-BASED FREQUENCY-RESPONSE FUNCTION IDENTIFICATION

With this study, a method for the experimental Frequency Response function identification is proposed. As discussed in Sec. 2.1, the receptance matrix $\hat{\alpha}(\omega)$, estimated from experiments, can be determined using Eq. (5). In Eq. (6), the spectrum of the excitation input $\hat{Y}(\omega)$ and of the structure response $\hat{X}(\omega)$ are determined from the ArUco marker centre displacement time histories $C_y(t)$ and $C_x(t)$ (see Eq. 8):

$$\widehat{Y_C}(\omega) = \int_{-\infty}^{\infty} C_y(t) \ e^{-i\omega t} \ dt \tag{10}$$

$$\widehat{X_C}(\omega) = \int_{-\infty}^{\infty} C_x(t) \ e^{-i\omega t} \ dt \tag{11}$$

Then, the receptance $\hat{\alpha}(\omega)$ is estimated using:

$$\hat{\alpha}(\omega) = \frac{\widehat{Y_C^*}(\omega) \ \widehat{X_C}(\omega)}{\widehat{Y_C^*}(\omega) \ \widehat{Y_C}(\omega)} \tag{12}$$

Finally, FRFs reconstruction using LSFD and LSCF approaches is performed.

4. EXPERIMENTAL RESEARCH

4.1. Setup

In this research, a Y-shaped specimen, shown in Figure 2, was used [4], [12]. In particular, this geometry was chosen due to its structural dynamic properties. In fact, by using two steel weights (each of 360 g), fixed to each of the arms, the structural dynamics were adjusted to the research needs. The Y-shaped sample was realised in White PLA, using an Ultimaker3 3D printer (100%
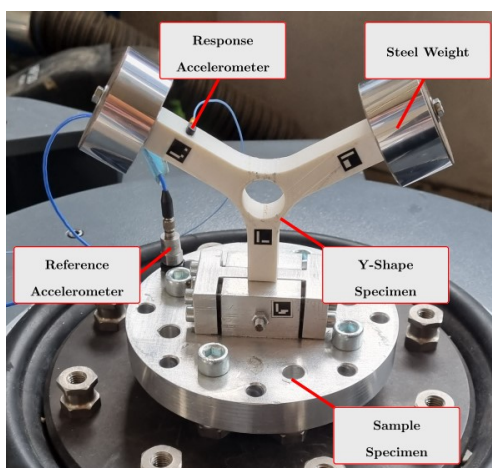
Figure 2. Y-shaped specimen with installed sensors.

Table 1. Technical specifications of accelerometers used.

Specifications	PCB-352C34	PCB-352C23/NC
Sensitivity	100 mV/g (±10 %)	5 mV/g (±20 %)
Measurement Range	±490 m/s² pk	±9810 m/s² pk
Frequency Range (±5 %)	0.5 to 10000 Hz	2 to 10000 Hz
Resonant Frequency	≥50 kHz	≥70 kHz
Broadband Resolution	0.0015 m/s² rms	0.03 m/s² rms
Non-Linearity	≥ 1 %	≥ 1 %
Transverse Sensitivity	≥ 5 %	≥ 5 %

infill and 0.1 mm of layer height). Default values for other printing parameters were used. In the printing process, three 8x8 mm² ArUco markers were embedded in the last four layers of the Y-sample geometry and printed using Black PLA material in one printing process (see Figure 2). The sample was mounted on an electro-dynamical shaker (Sentek L1024 with PA115 Power Amplifier), as shown in Figure 3. On the shaker fixation, a fourth ArUco marker (printed in b&w on a standard 80 g/m² paper in 8x8 mm²) was rigidly glued for the input excitation measurement. The marker detection was performed using a FLIR Backfly S 5 MP monochrome camera with Sony IMX250 sensor and Fujinon 12 mm optic mounted. The resolution of the camera was settled at 1000×850 pixels and the frame rate at 160 fps. The setup consists also of a PCB-352C34 accelerometer, bonded on the shaker fixation for controlling and measuring the input excitation, and of a PCB-352C23/NC, fixed on one Y-sample arm for the response measurement. The main specifications of the accelerometers used are shown in Table 1.

For the excitation, a sine-sweep of 0.5 g of constant amplitude from 5 Hz to 80 Hz was given to the shaker (close-loop control), with a sweep-rate of 16 Oct/min (i.e., approximately 4 sweeps in 68 seconds). The sweep rate was carefully chosen in order to excite the natural frequencies of the sample. However, the measurement with the camera was limited at approximately 45 seconds due to hardware and memory limitations.

4.2. Data acquisition

The marker used in this research are from the ArUco Original library, identified as shown in Figure 4. In particular, the markers with ID1 and ID7 are considered as input reference while the markers on the two arms (i.e., ID2 and ID5) as output displacement. The displacement of the four markers centre point, captured during the experiment and evaluated using Eq. 8 and Eq. 9, is shown in Figure 5.

Figure 3. Experimental setup.
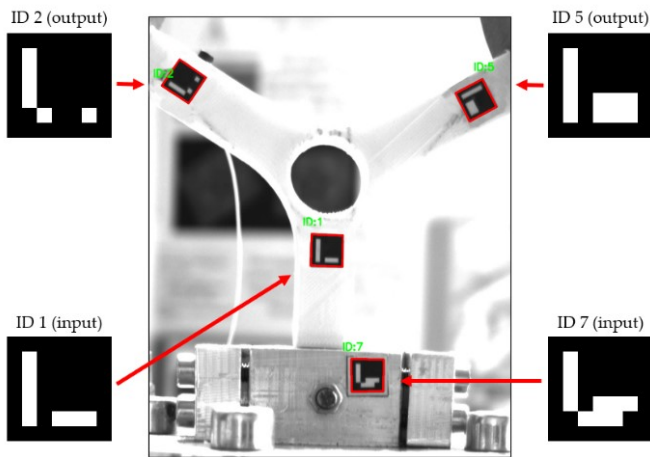
Figure 4. ArUco markers employed.
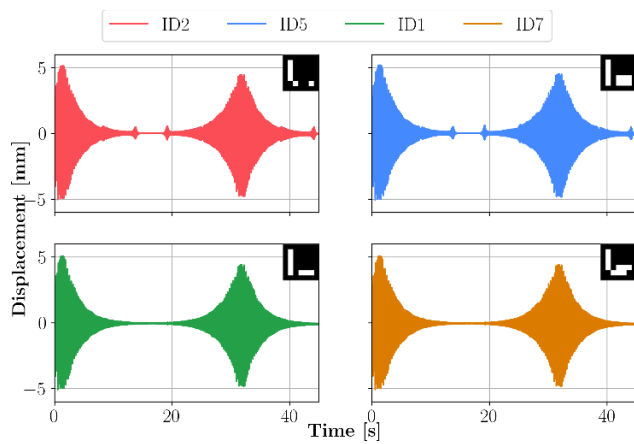
Figure 5. Measured displacement of the detected markers.

Once the displacement time-histories are obtained, the FRFs can be evaluated through Eq. 12, and, finally, reconstructed using LSFD and LSCF approaches. Similarly, the reference and the response accelerations time-histories are measured during the excitation (see Figure 6) and the acceleration FRF is evaluated [2].

4.3. Finite Element model

A finite element model of the Y-shaped specimen is prepared using a commercial software. Figure 7 shows the realized numerical model.

The structure has been meshed using solid element with ten degree of freedom for node for a total of 89962 elements and 131580 nodes. To model the external masses attached to the free end of the structures, two-point mass, with a mass equal to 0.36 kg each one, are rigidly connected to the holes on the arms of the structure. Moreover, to accurately replicate the experimental test, an additional mass of 1000 kg (namely *large mass* in Figure 7) was connected to the constrain zone of the structure. The displacement along the Y axis was not constrained, while all the other degree of freedom were fixed. In such a way it was possible to use the Large Mass Method to evaluate the frequency response both in terms of displacement and in terms of acceleration.

To calculate the numerical frequency response function (Shown in Sec. 5 the modal approach was used. For this reason, a modal analysis was necessary to obtain the natural frequencies of the system and the modal shapes in the point where the responses should be addressed. All the frequency response
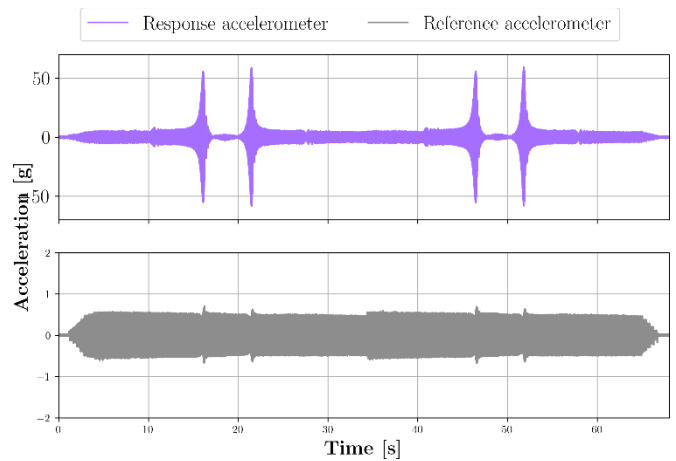
Figure 6. Reference and response accelerations.
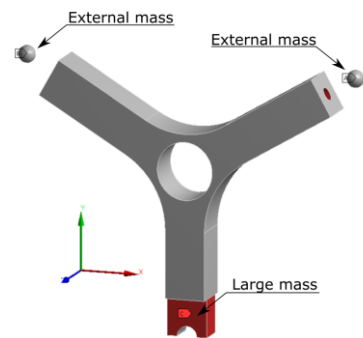
Figure 7. FE model of the Y-shaped specimen.

function shown in Sec. 5 were obtained considering a percentage damping equal to 1% constant for each vibrating mode.

5. RESULTS

Four different FRFs are obtained from the combination of the two markers as input and the two as output. However, as expected, the displacement measured with ID1 and ID7 markers is totally comparable and the same consideration can be performed for ID2 and ID5 markers, due to geometrical considerations. Due to this, for the sake of clarity, only ID1-ID2 markers FRF will be shown and considered in the further discussion.

From the results in Figure 8, the goodness of the numerical model is verified, comparing the FRF obtained performing the accelerometer-base experiments.
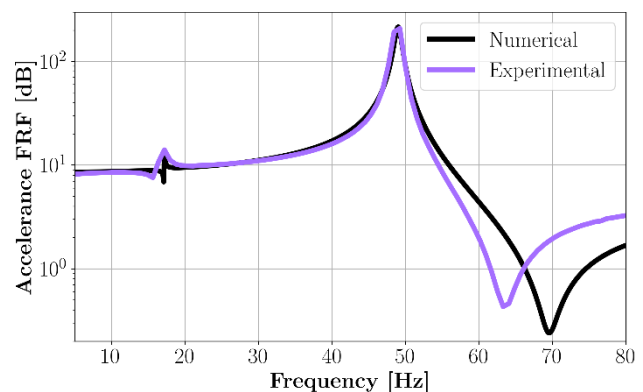
Figure 8. Experimental and numerical acceleration Frequency Response Functions comparison.
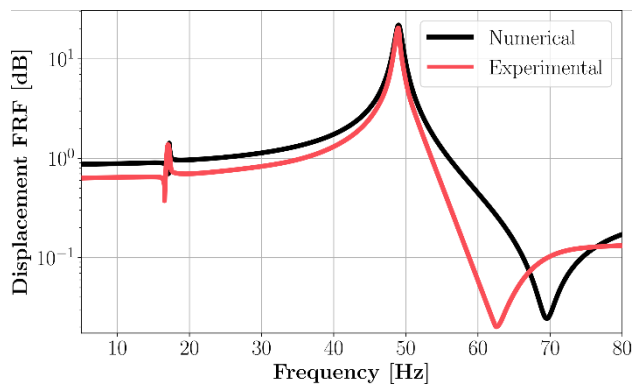
Figure 9. Experimental and numerical displacement Frequency Response Functions comparison.

Table 2. Natural frequencies obtained for each technique used. The standard deviation on each value is ±1.28 Hz.

Technique	1st Mode Frequency / Hz	2nd Mode Frequency / Hz	3rd Mode Frequency / Hz
ArUco markers	17.2	48.9	64.00
Accelerometers	17.2	49.0	63.9
Numerical model	17.2	48.9	69.5

In the considered frequency range, three predominant natural frequencies are clearly identified at approximately 17 Hz, 48 Hz and 69 Hz from both experiments and numerical model.

Finally, the comparison between the verified numerical model and the proposed approach is performed in terms of displacement FRF (see Figure 9).

In the same considered frequency range, the same natural frequencies are identified using the ArUco markers with high accuracy. The obtained natural frequencies are presented in Table 2.

A slightly decreasing of the third natural frequency is detected with respect to the numerical model. However, the experimental approaches give similar results, and this deviation can be attributed to the numerical model setting.

6. CONCLUSIONS

This study researches the modal components identification using a non-contact measurement approach based on ArUco marker displacement detection. Even though the established full-contact methods are widely used for several research applications, the required instrumentation is expensive and delicate, and the experimental procedures are time consuming for a full-field comprehensiveness of the dynamics of a structure. On the other hand, the proposed method proved high accuracy on the assessment of natural frequencies of a structure with a relatively low computational effort and extremely lower budget sensors instrumentation: each ArUco marker can be considered as a sensor, and if multiple markers are placed and detected in the field of view of the camera, more information on the dynamics of the structure can be easily provided. Moreover, using the 3D printing technology, embedded sensors are demonstrated to be effective and reliable. Further employment of ArUco markers in structural dynamics will be investigated.

REFERENCES

[1] D. Benasciutti, Fatigue analysis of random loadings. A frequency-domain approach, PhD University of Ferrara, Department of Engineering, 2004.

[2] J. Slavič, M. Boltezar, M. Mrsnik, M. Cesnik, J. Javh, Vibration Fatigue by Spectral Methods. Elsevier, 2021.
DOI: 10.1016/C2019-0-04580-3.

[3] D. Benasciutti, R. Tovo, Spectral methods for lifetime prediction under wide-band stationary random processes, Int J Fatigue, vol. 27, no. 8, Aug. 2005, pp. 867–877.
DOI: 10.1016/j.ijfatigue.2004.10.007

[4] L. Capponi, M. Česnik, J. Slavič, F. Cianetti, M. Boltežar, Non-stationarity index in vibration fatigue: Theoretical and experimental research, Int J Fatigue, vol. 104, Nov. 2017, pp. 221–230.
DOI: 10.1016/j.ijfatigue.2017.07.020

[5] M. Mršnik, J. Slavič, M. Boltežar, Vibration fatigue using modal decomposition, Mech Syst Signal Process, vol. 98, Jan. 2018, pp. 548–556.
DOI: 10.1016/j.ymssp.2017.03.052

[6] D. J. Ewins, Modal testing: theory and practice, vol. 15, Letchworth: Research studies press, 1984.

[7] Z.-F. Fu, J. He, Modal analysis. Elsevier, 2001.

[8] N. M. M. Maia, J. M. M. e Silva, Theoretical and experimental modal analysis. Research Studies Press, 1997.

[9] W. Heylen, S. Lammens, P. Sas, Modal analysis theory and testing, vol. 200, no. 7. Katholieke Universiteit Leuven Leuven, Belgium, 1997.

[10] T. Tocci, L. Capponi, R. Marsili, G. Rossi, Optical-flow-based motion compensation algorithm in thermoelastic stress analysis using single-infrared video, ACTA IMEKO, vol. 10, no. 4, Dec. 2021, p. 169.
DOI: 10.21014/acta_imeko.v10i4.1147

[11] F. Vurchio, G. Fiori, A. Scorza, S. A. Sciuto, Comparative evaluation of three image analysis methods for angular displacement measurement in a MEMS microgripper prototype: a preliminary study, ACTA IMEKO, vol. 10, no. 2, Jun. 2021, p. 119.
DOI: 10.21014/acta_imeko.v10i2.1047.

[12] L. Capponi, J. Slavič, G. Rossi, M. Boltežar, Thermoelasticity-based modal damage identification, Int J Fatigue, vol. 137, Aug. 2020, p. 105661.
DOI: 10.1016/j.ijfatigue.2020.105661.

[13] J. Javh, J. Slavič, M. Boltežar, Experimental modal analysis on full-field DSLR camera footage using spectral optical flow imaging, J Sound Vib, vol. 434, 2018, pp. 213–220.

[14] B. D. Lucas, T. Kanade, An iterative image registration technique with an application to stereo vision, Proceedings DARPA Image Understanding Workshop, 1981, pp. 121–130.

[15] D. Gorjup, J. Slavič, M. Boltežar, Frequency domain triangulation for full-field 3D operating-deflection-shape identification, Mech Syst Signal Process, vol. 133, Nov. 2019, p. 106287.
DOI: 10.1016/j.ymssp.2019.106287

[16] L. Capponi, Thermoelasticity-based analysis: collection of python packages. 2020.
DOI: 10.5281/ZENODO.4043102

[17] D. G. Lowe, Object recognition from local scale-invariant features, in Proceedings of the seventh IEEE international conference on computer vision, 1999, vol. 2, pp. 1150–1157.

[18] G. Allevi, L. Casacanditella, L. Capponi, R. Marsili, G. Rossi, Census Transform Based Optical Flow for Motion Detection during Different Sinusoidal Brightness Variations, J Phys Conf Ser, vol. 1149, no. 1, Dec. 2018, p. 012032.
DOI: 10.1088/1742-6596/1149/1/012032

[19] T. Tocci, L. Capponi, R. Marsili, G. Rossi, J. Pirisinu, Suction system vapour velocity map estimation through SIFT-based alghoritm, J Phys Conf Ser, vol. 1589, no. 1, Jul. 2020, p. 012004.
DOI: 10.1088/1742-6596/1589/1/012004

[20] T. Khuc, F. N. Catbas, Computer vision-based displacement and vibration monitoring without using physical target on structures, in Bridge Design, Assessment and Monitoring, Routledge, 2018, pp. 89–100.
DOI: 10.1201/9781351208796-8

[21] C.-Z. Dong, O. Celik, F. N. Catbas, Marker-free monitoring of the grandstand structures and modal identification using computer vision methods, Struct Health Monit, vol. 18, no. 5–6, Nov. 2019, pp. 1491–1509.
DOI: 10.1177/1475921718806895

[22] F. Lunghi, A. Pavese, S. Peloso, I. Lanese, D. Silvestri, Computer Vision System for Monitoring in Dynamic Structural Testing, in Role of seismic testing facilities in performance-based earthquake engineering, vol. 22, M. N. Fardis and Z. T. Rakicevic, Eds. Dordrecht: Springer Netherlands, 2012, pp. 159–176.
DOI: 10.1007/978-94-007-1977-4

[23] S. W. Park, H. S. Park, J. H. Kim, H. Adeli, 3D displacement measurement model for health monitoring of structures using a motion capture system, Measurement, vol. 59, Jan. 2015, pp. 352–362.
DOI: 10.1016/j.measurement.2014.09.063

[24] F. J. Romero-Ramirez, R. Muñoz-Salinas, R. Medina-Carnicer, Speeded up detection of squared fiducial markers, Image Vis Comput, vol. 76, Aug. 2018, pp. 38–47.
DOI: 10.1016/j.imavis.2018.05.004

[25] S. Garrido-Jurado, R. Muñoz-Salinas, F. J. Madrid-Cuevas, M. J. Marín-Jiménez, Automatic generation and detection of highly reliable fiducial markers under occlusion, Pattern Recognit, vol. 47, no. 6, Jun. 2014, pp. 2280–2292.
DOI: 10.1016/j.patcog.2014.01.005

[26] L. Capponi, T. Tocci, M. D'Imperio, S. H. Jawad Abidi, M. Scaccia, F. Cannella, R. Marsili, G. Rossi, Thermoelasticity and ArUco marker-based model validation of polymer structure: application to the San Giorgio's bridge inspection robot, ACTA IMEKO, vol. 10, no. 4, Dec. 2021, p. 177.
DOI: 10.21014/acta_imeko.v10i4.1148

[27] N. Elangovan, A. Dwivedi, L. Gerez, C.-M. Chang, M. Liarokapis, Employing IMU and ArUco Marker Based Tracking to Decode the Contact Forces Exerted by Adaptive Hands, in 2019 IEEE-RAS 19th International Conference on Humanoid Robots (Humanoids), Oct. 2019, pp. 525–530.
DOI: 10.1109/Humanoids43949.2019.9035051

[28] M. F. Sani, G. Karimian, Automatic navigation and landing of an indoor AR. drone quadrotor using ArUco marker and inertial sensors, in 2017 International Conference on Computer and Drone Applications (IConDA), Nov. 2017, pp. 102–107.
DOI: 10.1109/ICONDA.2017.8270408

[29] I. Lebedev, A. Erashov, A. Shabanova, Accurate Autonomous UAV Landing Using Vision-Based Detection of ArUco-Marker, in International Conference on Interactive Collaborative Robotics, Springer, 2020, pp. 179–188.
DOI: 10.1007/978-3-030-60337-3_18

[30] M. Abdelbarr, Y. L. Chen, M. R. Jahanshahi, S. F. Masri, W.-M. Shen, U. A. Qidwai, 3D dynamic displacement-field measurement for structural health monitoring using inexpensive RGB-D based sensor, Smart Mater Struct, vol. 26, no. 12, Dec. 2017, p. 125016.
DOI: 10.1088/1361-665X/aa9450

[31] M. Kalybek, M. Bocian, N. Nikitas, Performance of Optical Structural Vibration Monitoring Systems in Experimental Modal Analysis, Sensors, vol. 21, no. 4, Feb. 2021, p. 1239.
DOI: 10.3390/s21041239

[32] T. Tocci, L. Capponi, G. Rossi, ArUco marker-based displacement measurement technique: uncertainty analysis, Engineering Research Express, vol. 3, no. 3, Sep. 2021, p. 035032.
DOI: 10.1088/2631-8695/ac1fc7

[33] P. Guillame, B. Peeters, B. Cauberghe, P. Verboven, Identification of highly damped systems and its application to vibro-acoustic modeling, 2004.

[34] P. Guillaume, P. Verboven, B. Cauberghe, S. Vanlanduit, E. Parloo, G. de Sitter, Frequency-Domain System Identification Techniques for Experimental and Operational Modal Analysis, IFAC Proceedings Volumes, vol. 36, no. 16, Sep. 2003, pp. 1609–1614.
DOI: 10.1016/S1474-6670(17)34990-X

[35] B. Peeters, H. van der Auweraer, P. Guillaume, J. Leuridan, The PolyMAX Frequency-Domain Method: A New Standard for Modal Parameter Estimation?, Shock and Vibration, vol. 11, no. 3–4, 2004, pp. 395–409.
DOI: 10.1155/2004/523692